graft polymerization was conducted in this study to covalently link the poly(MPTS) and the substrate, that is, to obtain a permanently modified surface. Prior to the graft polymerization, the substrate surface was first modified with 3-mercaptopropyltrimethoxysilane, which has mercapto groups. A mercapto group has a large transfer coefficient for radicals [29], which results in the formation of sulfur radicals on the substrate in the presence of a free-radical initiator such as AIBN. The silanization and the graft polymerization onto the stainless-steel substrate were conducted based on literature [27].

Table 1 shows the surface composition of the original, silanized, and poly(MPST)-grafted stainless-steel substrates measured by XPS. The XPS spectrum of the original substrate showed carbon and oxygen signals in addition to metal signals. The carbon signal could be attributed to the intrinsic carbon content of the steel alloy and/or the adsorption of trace amounts of hydrocarbon contaminants on the substrates. The strong O_{1s} signal in the original substrate could be attributed to hydrated oxides that covered common metals and alloys under ambient conditions. The presence of the hydrated oxides is favorable for the subsequent silanization because the coupling of a silane compound on a metal surface is considered to involve the following three steps [30, 31]: (1) hydrolysis of the silane coupling agents; (2) formation of hydrogen bonding; and (3) formation of metal-oxide bonding (M-O-Si). After the silanization of the substrate, the corresponding silicone and sulfur signals were observed in the XPS spectrum with an enhanced C_{1s} signal. The presence of metal signals suggests the formation of a thin layer of the silane coupling agent on the substrate. Following the graft polymerization of MPTS, the metal signals were not observed by XPS, suggesting the formation of a thick and uniform coating of the

poly(MPTS) on the substrate.

Fig. 3 shows the ATR FT-IR spectra of the MPTS homopolymer produced by solution polymerization under the same conditions as those in the graft polymerization, and the stainless-steel surface after the graft polymerization of MPTS. The spectrum of the MPTS homopolymer was measured after dip coating on the original stainless-steel substrate with its ethanol solution. It is noteworthy that the spectrum of the original stainless-steel substrate did not show any peaks in the same range. In the case of the MPTS homopolymer physically adsorbed on the original substrate, the Si-O-C stretching vibration of the alkoxysilyl groups was observed at 1076 cm^{-1}. On the other hand, in the case of the substrate after the graft polymerization of MPTS, the same spectrum as that in the poly(MPST) was observed. It is important to note that the poly(MPST) spectrum was observed on the grafted substrate after vigorous washing with ethanol, although the spectrum of the MPTS homopolymer physically adsorbed on the substrate disappeared after one wash with ethanol. From the above results, it was clear that the grafting of poly(MPTS) from the stainless-steel surface was well conducted.

The HAp nanocrystals, which were calcined at 800°C, were coated on the poly(MPTS)-grafted substrate through covalent linkage. Fig. 4 shows the SEM photographs of the HAp-coated substrate after ultrasonic washing. As a negative control, the original substrate, which was neither modified with the silane coupling agent nor with MPTS, was used for the modification with HAp nanocrystals. Although the HAp nanocrystals were adsorbed on the original substrate, nearly all of them were removed by the ultrasonic treatment, as shown in Fig. 4 (b). On the other hand, the crystals remained on the poly(MPTS)-grafted surface, regardless of the

morphology (spherical or rod-shaped) of the HAp crystals. The substrate was uniformly covered by the HAp nanocrystals without severe aggregations, because nearly all the nanocrystals could be dispersed in a medium by preventing the calcination-induced sintering among the crystals with the anti-sintering agent [24, 25]. Since the covalent linkage could not be observed directly on the substrate, the covalent linkage was estimated indirectly from the FT-IR analysis for the mixture of the HAp nanocrystals and MPTS homopolymer [7]. Contact atomic force microscopy also revealed that the bonding strength between the HAp nanocrystal and the poly(MPTS)-grafted surface was approximately 12 times higher than that of the original surface. The relationship between the nature of the surface and the bonding strength will be discussed in a separate publication [32].

Figs. 5 and 6 show the SEM photographs of HUVEC morphologies and the number of HUVEC on the samples after 24 h of incubation. The cover ratio of the HAp/stainless steel was controlled at around 50% by changing the concentration of HAp dispersion in the adsorption process. The cells seldom adhered on the original substrate for such a short period of incubation. On the other hand, the number of cells that adhered on the HAp-coated substrates was larger than that in the case of the original substrate (see Fig. 6). Kilpadi *et al.* showed that cell-adhesion proteins such as fibronectin and vitronectin exhibited significantly improved adsorption on HAp ceramic discs sintered at 1000°C for 3 h than on Type 316L stainless steel; this leads to the conclusion that integrins (fibronectin-binding integrin, $\alpha_5\beta_1$; vitronectin-binding integrin, $\alpha_v\beta_3$) and osteoblast precursor cells adhere significantly better on the HAp disc [33]. These observations suggest that the improved integrin-mediated cell binding may be one of the mechanisms that lead

to better cell adhesion on the HAp-coated substrates. As compared to TCPS, HUVEC on the HA-coated substrates spread to a greater extent and had pavement-like monolayer morphologies, as shown in Fig. 5. The number of cells on the HA-coated substrates, however, was lesser than that on TCPS (see Fig. 6). Although the cause of this phenomenon is unclear at present, it may be based on the more preferential adhesion of cell-adhesion proteins on the HAp-coated substrates than on TCPS, and/or the surface topography of the HAp-coated substrate, as discussed below.

Next, the influence of the HAp morphology was evaluated. As indicated above, fibronectin and vitronectin are important for cell adhesion, and these acidic proteins expected to adhere better to the *a*-plane surface of HAp; in other words, they adhere better to the rod-shaped HAp crystals elongated along their *c*-axis [25] than on spherical HAp. However, there was no difference between the number of cells and the degree of cell spreading (see Fig. 5) in the rod-shaped and the spherical HAp-coated substrates having the same surface cover ratio of HAp (50%) under the present conditions. These results suggest that the cell adhesion on a nano-sized HAp-coated surface is affected by not only the chemistry of HAp but also the surface topography such as degree of roughness and microdomain structure: cell adhesion, proliferation, and detachment strength were surface-roughness sensitive and increased with the roughness of HAp [35]; and the structure and size of the phase-separated microdomains on the block copolymer, the blocks of which had different protein adhesion properties, influenced the cell adhesion due to "capping control" of the membrane proteins on the cells [36, 37]. The topography control of HAp nanocrystal coating, such as the orientation of HAp nanocrystals and the distance between the nanocrystals on the surface, are now being attempted, and the cell-adhesion behavior on the

controlled surface will be reported in the near future.

The HAp nanocrystal coating technique is also applicable to materials with complex shapes since it is a solution process. We coated a stent (made of Type 316L stainless steel; ACTMENT Co. Ltd., Japan) with HAp nanocrystals by using the procedures described above (Fig. 7); we are now evaluating it through *in vivo* animal implantation experiments. Although Type 316L stainless-steels play a key role in metal biomaterials due to their excellent mechanical features, low cost, and ease of fabrication, they fail miserably in *in vivo* conditions due to corrosion-related problems [38] such as nickel-contact allergy [39]. Köster *et al.* have reported that patients with allergic patch-test reactions to nickel and molybdenum showed a higher frequency of in-stent restenosis than patients without hypersensitivity in a retrospective study [40], this observation suggests that allergic reactions to nickel and molybdenum ions released from stainless-steel stents may be one of the triggering mechanisms for in-stent restenosis. The HAp nanocrystal coating technique developed in this article is expected to retard the corrosion of metals because this method involves the uniform coating of the polymer layer on the metal surface.

Conclusion

A novel technique for coating Type 316L stainless-steel substrate with calcined HAp nanocrystals through covalent linkage without high-temperature treatment was developed. The coating involved three steps: (1) silanization of the substrate at 110°C; (2) graft polymerization of poly(MPTS), which could react with HAp crystals, at 70°C; (3) adsorption of HAp

nanocrystals on the substrate and reaction with alkoxyl groups in the grafted polymer on the substrate at 80°C. In a cell-adhesion test, HUVEC adhered in larger numbers on the HAp-coated substrate as compared with the original one, and spread to a greater extent than that on TCPS after 24 h of initial incubation. The number of cells that adhered and the degree of cell spreading were not different for the rod-shaped and the spherical HAp coating in the present conditions. The HAp nanocrystal coating technique is an effective way to improve the cell affinity of metal materials because it is a coating method that does not involve high-temperature treatment, and it can be applied to materials with complex shapes since it is a solution process.

5. Acknowledgment

This work was supported by a Research Grant for Cardiovascular Diseases from the Ministry of Health, Labour and Welfare, Japan.

6. References

1. Jarcho M. Calcium phosphate ceramics as hard tissue prosthetics. Clin Orthop 1981;157: 259-278.
2. Jarcho M. Retrospective analysis of hydroxyapatite development for oral implant applications. Dent Clin North Am 1992;36:19-26.
3. De Bruijn JD, Van Blitterswijk CA, Davies JE. Initial bone matrix formation at the hydroxyapatite interface in vivo. J Biomed Mater Res 1995;29: 89-99.
4. Okumura M, Ohgushi H, Dohi Y, Katuda T, Tamai S, Koerten HK, Tabata S. Osteoblastic phenotype expression on the surface of hydroxyapatite ceramics. J Biomed Mater Res 1997;37: 122-129.
5. Deligianni DD, Katsala ND, Koutsoukos PG, Missirlis YF. Effect of surface roughness of hydroxyapatite on human bone marrow cell adhesion, proliferation, differentiation and detachment strength. Biomaterials 2001;22: 87-96
6. Aoki H, Medical Applications of Hydroxyapatite, Tokyo and St. Louis, Ishiyaku EuroAmerica Inc., 1994.
7. Furuzono T, Kishida A, Tanaka J. Nano-scaled hydroxyapatite/polymer composite I. Coating of sintered hydroxyapatite particles on poly(γ-methacryloxypropyl trimethoxysilane)-grafted silk fibroin fibers through chemical bonding. J Mater Sci: Mater Med 2004;15:19-23.
8. T. Furuzono, S. Yasuda, T. Kimura, S. Kyotani, J. Tanaka, A. Kishida, Nano-scaled hydroxyapatite/polymer composite IV. Fabrication and cell adhesion properties of a three-dimensional scaffold made of composite material with a silk fibroin substrate to develop a percutaneous device, J Artif Organs 2004;7:137-144.
9. Furuzono T, Masuda M, Okada M, Yasuda S, Kadono H, Tanaka R, and Miyatake K. Increase of cell adhesiveness on poly(ethylene terephthalate) fabric by coating of sintered

hydroxyapatite nanocrystals for development of an artificial blood vessel, ASAIO J 2006;52: 315-320.

10. Furuzono T, Wang P, Korematsu A, Miyazaki K, Oido-Mori M, Kowashi Y, Ohura K, Tanaka J, Kishida A. Physical and biological evaluations of sintered hydroxyapatite/silicone composite with covalent bonding for a percutaneous implant material. J Biomed Mater Res B: Appl Biomater 2003;65B:217-226.
11. Disegi JA, Eschbach L. Stainless steel in bone surgery. Injury 2000;31:2-6.
12. Levesque J, Dube D, Fiset M, Mantovani D. Materials and properties for coronary stents. Adv Mater Process 2004;162:45-48.
13. Kangasniemi IOM, Verheyen CCPM, van der Velke EA, deGoot, K, In vivo tensile testing of fluorapatite and hydroxyapatite plasma-sprayed coatings, J Biomed Mater Res 1994;28:563-572.
14. Ong JL, Lucus LC, Lacefield WR, Rigney ED. Structure, solubility and bond strength of thin calcium phosphate coatings produces by ion beam sputter deposition. Biomaterials 1992;13:249-254.
15. Yoshinari M, Hayakawa T, Wolke JCG. Influence of rapid heating with infrared radiation on RF magnetron sputtered calcium phosphate coatings. J Biomed Mater Res 1997;37:60-67.
16. Wang CK, Lin JHC, Ju CP, Ong HC, Chang RPH. Structural characterization of pulsed laser-deposited hydroxyapatite film on titanium substrate. Biomaterials 1997;18:1331-1338.
17. Monma H. Electrochemical Deposition of Calcium-Deficient Apatite on Stainless Steel Substrate. J Ceram Soc Jpn 1993;101:737-739.
18. Sridhar TM, Subbaiyan M, Mudali UK. Preparation and characterisation of electrophoretically deposited hydroxyapatite coatings on type 316L stainless steel. Corros Sci 2003;45:237-252.

19. Mondragon-Cortez P, Vargas-Gutierrez G. Electrophoretic deposition of hydroxyapatite submicron particles at high voltages. Mater Lett 2004;58:1336-1339.

20. Kim DG, Shin MJ, Kim KH, Hanawa T. Surface treatments of titanium in aqueous solutions containing calcium and phosphate ions. Bio-Med Mater Eng 1999;9:89-96.

21. Balamurugan A, Kannan S, Rajeswari S. Electrochemical evaluation of sol-gel hydroxyapatite coatings on type 316L stainless steel-in vitro study. Can Metall Q 2004;43:293-296.

22. Ong JL, Lucas LC. Post-deposition heat treatment for ion beam sputter deposited calcium phosphate coatings. Biomaterials 1994;15:337-341.

23. Weiss B, Stickler R. Phase instabilities during high temperature exposure of 316 austenitic stainless steel. Metal Trans, 1972;3:851-866.

24. Filiaggi MJ, Pilliar RM. Interfacial characterization of a plasma-sprayed hydroxyapatite/Ti-6Al-4V implant system, in Transactions of the Tenth Annual Meeting of the Canadian Society for Biomaterials, pp.23-25 (1989)

25. Okada M, Furuzono T. Calcination of rod-like hydroxyapatite nanocrystals with an anti-sintering agent surrounding the crystals. J Nanoparticle Res, in press (Published Online at 22 July 2006)

26. Okada M, Furuzono T. Fabrication of high-dispersibility nanocrystals of calcined hydroxyapatite. J Mater Sci 2006;41: 6134-6137.

27. Zhang F, Kang ET, Neoh KG, Wang P, Tan KL. Surface modification of stainless steel by grafting of poly(ethylene glycol) for reduction in protein adsorption. Biomaterials 2001;22:1541-1548.

28. Nishizawa K, Suzuki T, Kawamoto Y, Toriyama M, Yokogawa Y, Nagata F, Tai Y, Kameyama T. Surface modification of bioceramics by silane coupling agent and their

evaluation. J Chem Soc Jpn 1998;106:709-714.

29. Brandrup J, Immergut EH (eds), Polymer Handbook 3rd Edition, Wiley and Sons Inc., New York, 1989

30. Pluedemann EP (ed), Silane coupling agent, Plenum Press, New York, 1991.

31. Mittal KL (ed), Silane and other coupling agents, VSP, Utrecht, 1992.

32. Okada M, Furukawa K, Serizawa T, Yanagisawa Y, Tanaka H, Kawai T, Furuzono T. Estimation of interfacial interaction strength between calcined hydroxyapatite nanocrystals and substrate surface, in preparation.

33. Kilpadi KL, Chang PL, Bellis SL. Hydroxylapatite binds more serum proteins, purified integrins, and osteoblast precursor cells than titanium or steel. J Biomed Mater Res 2001;57:258-267.

34. Kawasaki T, Niikura M, Kobayashi Y. Fundamental study of hydroxyapatite high-performance liquid chromatography III. Direct experimental confirmation of the existence of two types of adsorbing surface on the hydroxyapatite crystal. J Chromatogr A 1990;515:125-148.

35. Deligianni D D, Katsala N D, Koutsoukos P G, Missirlis Y F. Effect of surface roughness of hydroxyapatite on human bone marrow cell adhesion, proliferation, differentiation and detachment strength. Biomaterials 2001; 22: 87-96.

36. Okano T, Uruno M, Sugiyama N, Shimada M, Shinohara I, Kataoka K, Sakurai Y. Suppression of platelet activity on microdomain surfaces of 2-hydroxyethyl methacrylate-polyether block copolymers. J Biomed Mater Res 1986;20:1035-1047

37. Okano T, Kataoka K, Sakurai Y, Shimada M, Miyahara M, Akaike T, Shinohara I. Molecular design of block and graft copolymers having the ability to suppress platelet adhesion. Artif Organs 1981;5:468-470

38. Kannan S, Balamurugan A, Rajeswari S, Subbaiyan M. Metallic implants. An approach for long term applications in bone related defects. Corros Rev 2002;20:339-358.

39. Schnuch A, Geier J, Lessmann H, Uter W. Decrease in nickel sensitization in young patients--successful intervention through nickel exposure regulation? Results of IVDK, 1992-2001, Hautarzt 2003;54:626-632.

40. Köster R, Vieluf D, Kiehn M, Sommerauer M, Kahler J, Baldus S,Meinertz T, Hamm CW. Nickel and molybdenum contact allergies in patients with coronary in-stent restenosis. Lancet 2000;356:1895-1897.

Table 1 Atomic percentages of the surfaces of the stainless-steel substrates evaluated by X-ray photoelectron spectroscopy

	C	O	Si	S	Cr	Fe	Ni
Original	25.9	50.9	0.6	0.4	10.6	5.0	1.0
Silized	35.0	44.4	2.5	1.9	9.3	5.0	0.6
Poly(MPTS)-Grafted	68.2	27.0	4.8	-	-	-	-

Figure captions

Fig. 1 Schematic process diagram of HAp nanocrystal coating for stainless-steel substrate through covalent linkage.

Fig. 2 SEM photographs of (a) spherical and (b) rod-shaped HAp nanocrystals prepared by wet chemical process followed by calcination at 800°C with anti-sintering agent.

Fig. 3 ATR FT-IR spectra of (a) poly(γ-methacryloxypropyl trimethoxysilane) prepared by solution polymerization and (b) the surface of stainless-steel substrate after the graft polymerization.

Fig. 4 SEM photographs of the surfaces of (a) the original stainless-steel substrate and (b–d) the substrates after the HAp nanocrystal coating followed by ultrasonic washing. Poly(MPTS)-grafting: (a, b) nonexistence; (c, d) existence. HAp nanocrystals: (b, c) spherical; (d) rod-shaped.

Fig. 5 SEM photographs of HUVEC adhering on (a) the original, (b) tissue culture polystyrene (TCPS), (c) spherical HAp-coated, and (d) rod-shaped HAp-coated stainless-steel substrates after incubation in 24-well multiplates (8×10^4 cells/cm^2) at 37°C for 24 h.

Fig. 6 Number of HUVEC adhering on (a) the original, (b) spherical HAp-coated, and (c) rod-like HAp-coated stainless-steel substrates after incubation in 24-well multiplates (8×10^4 cells/cm^2) at 37°C for 24 h. The number was normalized by the number of HUVEC that adhered on TCPS.

Fig. 7 Type 316L stainless-steel stent (a) before and (b) after coating with rod-shaped HAp nanocrystals, and (c) SEM photograph of the surface of the HAp-coated stent.

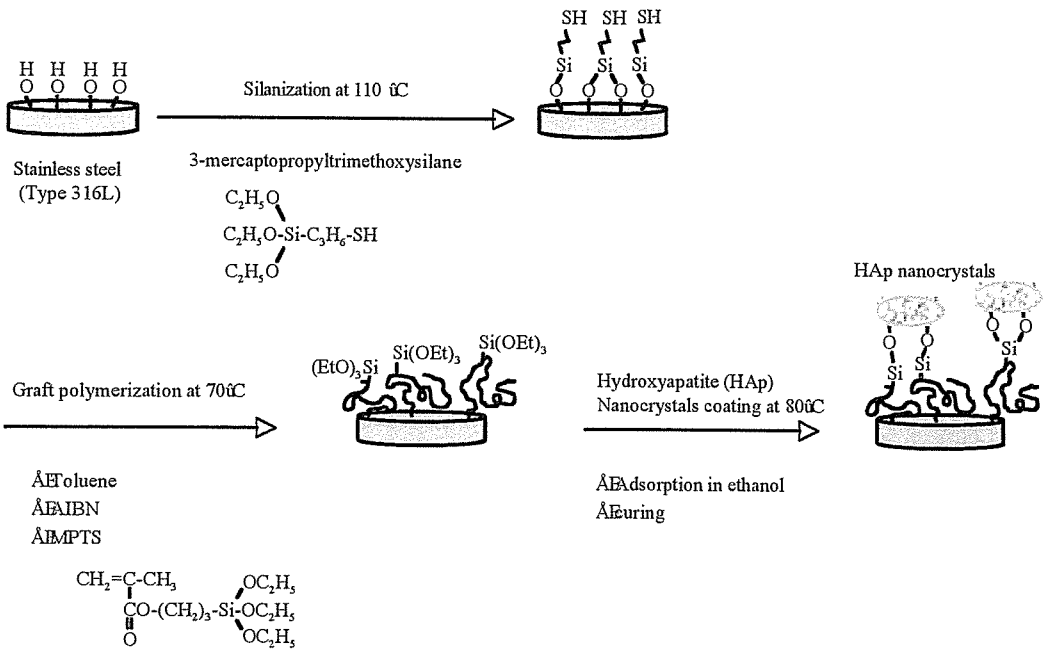

Fig. 1 Schematic process diagram of HAp nanocrystal coating for stainless-steel substrate through covalent linkage.

Fig. 1 Okada *et al.*

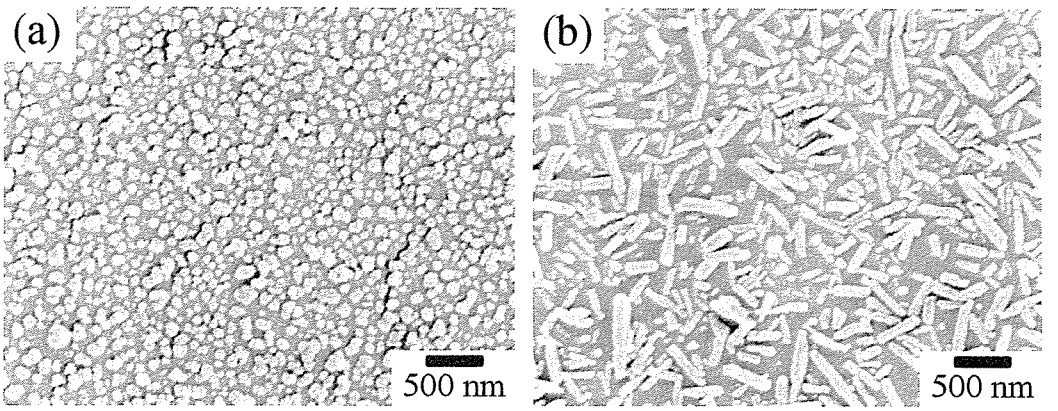

Fig. 2 SEM photographs of (a) spherical and (b) rod-shaped HAp nanocrystals prepared by wet chemical process followed by calcination at 800°C with anti-sintering agent.

Fig. 2 Okada *et al.*

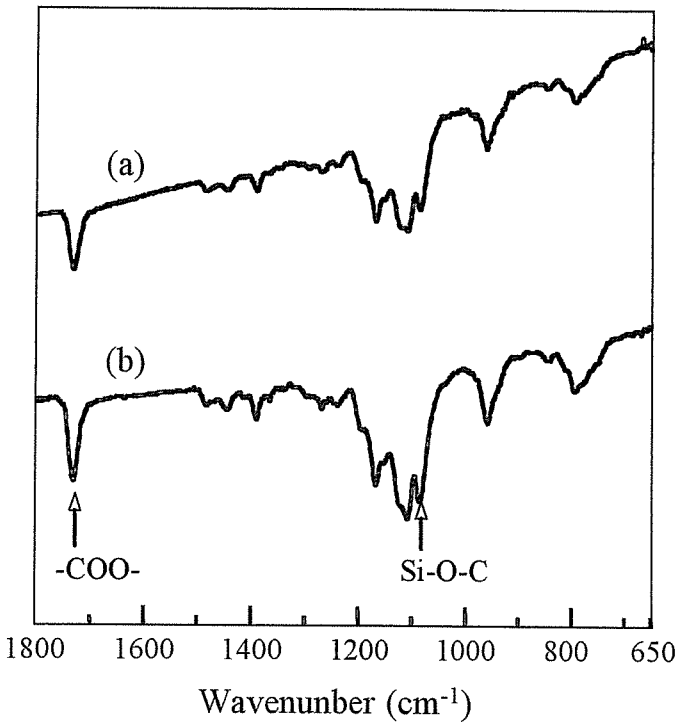

Fig. 3 ATR FT-IR spectra of (a) poly(γ-methacryloxypropyl trimethoxysilane) prepared by solution polymerization and (b) the surface of stainless-steel substrate after the graft polymerization.

Fig. 3 Okada *et al.*

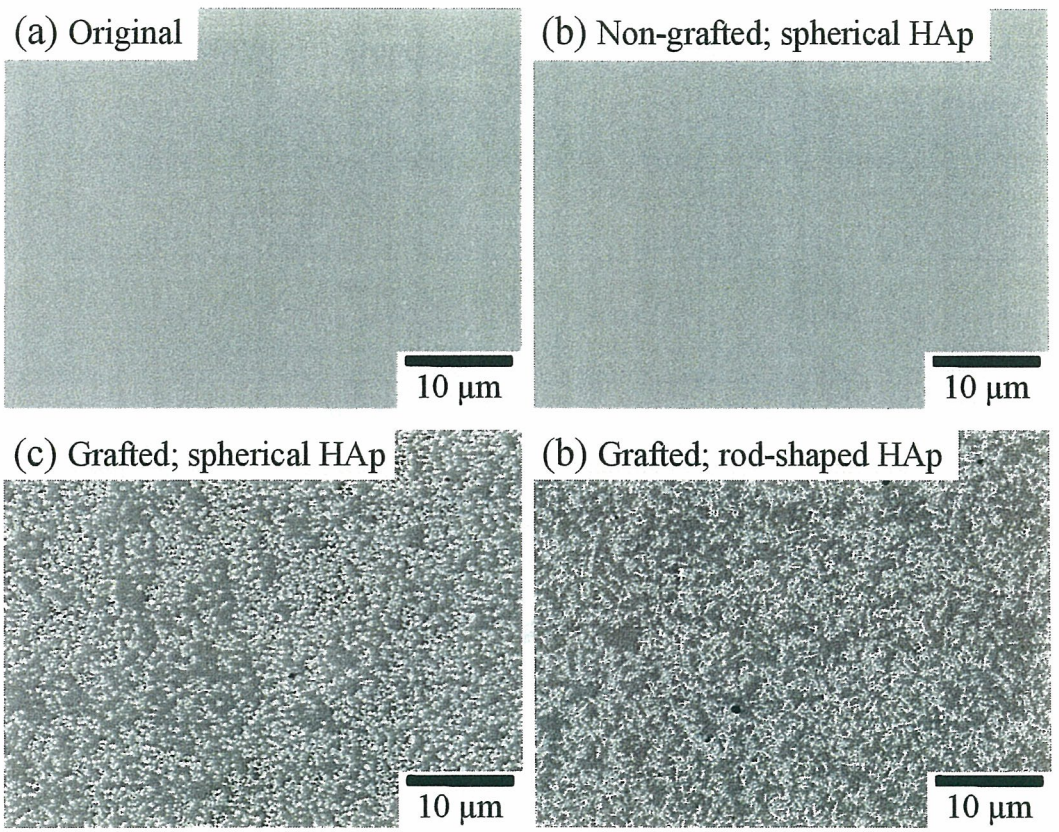

Fig. 4 SEM photographs of the surfaces of (a) the original stainless-steel substrate and (b–d) the substrates after the HAp nanocrystal coating followed by ultrasonic washing. Poly(MPTS)-grafting: (a, b) nonexistence; (c, d) existence. HAp nanocrystals: (b, c) spherical; (d) rod-shaped.

Fig. 4 Okada *et al.*

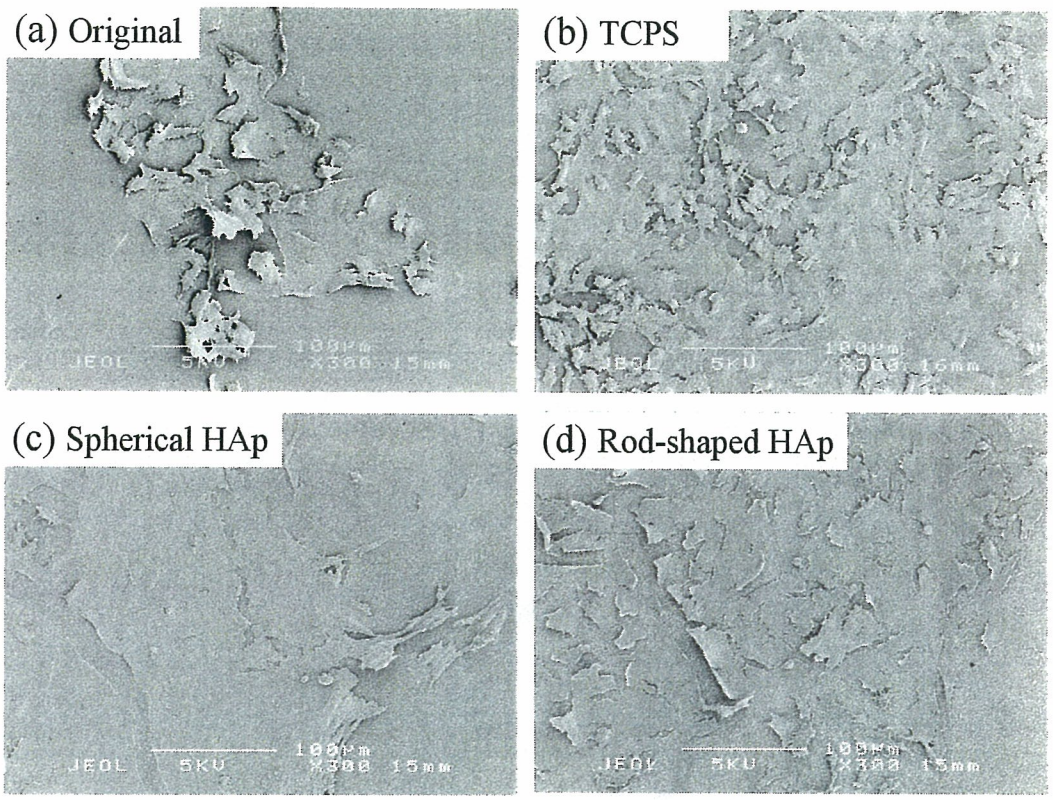

Fig. 5 SEM photographs of HUVEC adhering on (a) the original, (b) tissue culture polystyrene (TCPS), (c) spherical HAp-coated, and (d) rod-shaped HAp-coated stainless-steel substrates after incubation in 24-well multiplates (8×10^4 cells/cm^2) at 37°C for 24 h.

Fig. 5 Okada *et al.*

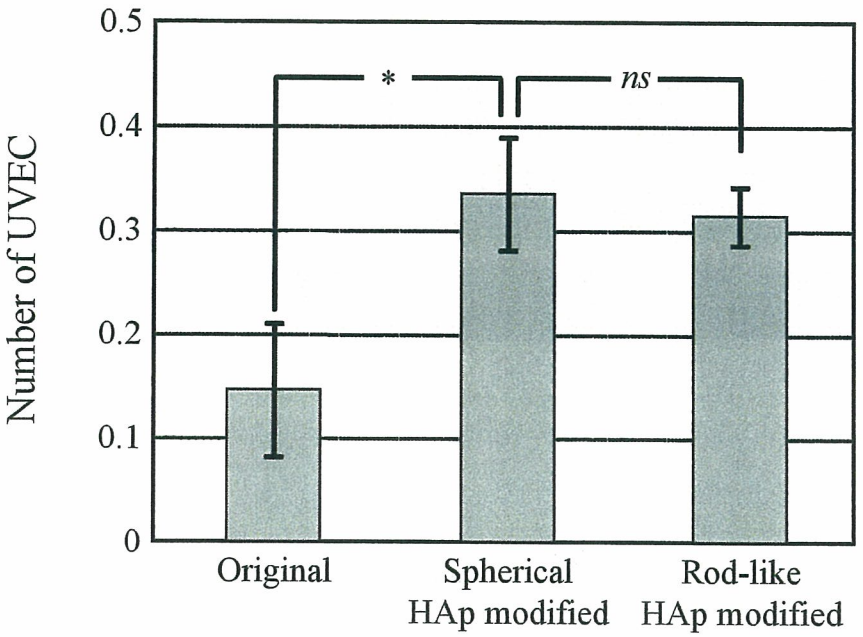

Fig. 6 Number of HUVEC adhering on (a) the original, (b) spherical HAp-coated, and (c) rod-like HAp-coated stainless-steel substrates after incubation in 24-well multiplates (8×10^4 cells/cm^2) at 37°C for 24 h. The number was normalized by the number of HUVEC that adhered on TCPS.

Fig. 6 Okada *et al.*

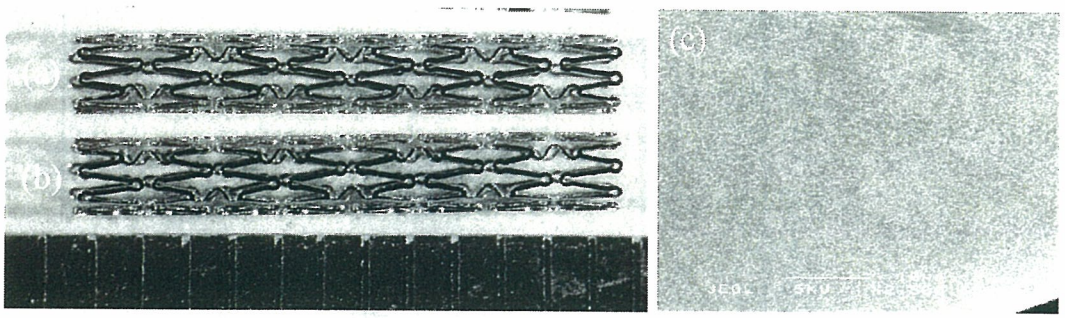

Fig. 7 Type 316L stainless-steel stent (a) before and (b) after coating with rod-shaped HAp nanocrystals, and (c) SEM photograph of the surface of the HAp-coated stent.

Fig. 7 Okada *et al.*